International Journal of Nanomedicine

Dovepress

open access to scientific and medical research

Open Access Full Text Article

ORIGINAL RESEARCH

Magnesium Ion-Doped Mesoporous Bioactive Glasses Loaded with Gallic Acid Against Myocardial Ischemia/Reperfusion Injury by Affecting the Biological Functions of Multiple Cells

Wenpeng Yu[1–4,*], Jingli Ding[5,*], Jianfeng Chen[1–3,*], Ying Jiang[4], Jinping Zhao[1–3], Jichun Liu[4,6], Jianliang Zhou[1–3], Jinping Liu[1–3]

[1]Department of Cardiovascular Surgery, Zhongnan Hospital of Wuhan University, Wuhan, 430071, People's Republic of China; [2]Hubei Provincial Engineering Research Center of Minimally Invasive Cardiovascular Surgery, Wuhan, 430071, People's Republic of China; [3]Wuhan Clinical Research Center for Minimally Invasive Treatment of Structural Heart Disease, Wuhan, 430071, People's Republic of China; [4]Department of Cardiovascular Surgery, The Second Affiliated Hospital of Nanchang University, Nanchang, 330006, People's Republic of China; [5]Department of Gastroenterology, Zhongnan Hospital of Wuhan University, Wuhan, 430071, People's Republic of China; [6]Department of Cardiovascular Surgery, The First Affiliated Hospital of Nanchang University, Nanchang, 330006, People's Republic of China

*These authors contributed equally to this work

Correspondence: Jianliang Zhou; Jinping Liu, Department of Cardiovascular Surgery, Zhongnan Hospital of Wuhan University, 169 Donghu Road, Wuhan, 430071, People's Republic of China, Tel +86 13767117511; +86 27-67812888, Email zjl20210802@whu.edu.cn; liujinping@znhospital.cn

Introduction: Excessive generation of reactive oxygen species (ROS) following myocardial ischemia-reperfusion (I/R) can result in additional death of myocardial cells. The rapid clearance of ROS after reperfusion injury and intervention during subsequent cardiac repair stages are crucial for the ultimate recovery of cardiac function.

Methods: Magnesium-doped mesoporous bioactive glasses were prepared and loaded with the antioxidant drug gallic acid into MgNPs by sol-gel method. The antioxidant effects of MgNPs/GA were tested for their pro-angiogenic and anti-inflammatory effects based on the release characteristics of GA and Mg^{2+} from MgNPs/GA. Later, we confirmed in our in vivo tests through immunofluorescence staining of tissue sections at various time points that MgNPs/GA exhibited initial antioxidant effects and had both pro-angiogenic and anti-inflammatory effects during the cardiac repair phase. Finally, we evaluated the cardiac function in mice treated with MgNPs/GA.

Results: We provide evidence that GA released by MgNPs/GA can effectively eliminate ROS in the early stage, decreasing myocardial cell apoptosis. During the subsequent cardiac repair phase, the gradual release of Mg^{2+} from MgNPs/GA stimulated angiogenesis and promoted M2 macrophage polarization, thereby reducing the release of inflammatory factors.

Conclusion: MgNPs/GA acting on multiple cell types is an integrated solution for comprehensive attenuation of myocardial ischaemia-reperfusion injury and cardiac function protection.

Keywords: myocardial ischemia/reperfusion injury, mesoporous bioactive glass, gallic acid, magnesium ion, macrophage polarization

Introduction

Acute myocardial infarction is a significant cause of heart failure and mortality.[1] Early reperfusion therapy serves as a pivotal strategy in the treatment of myocardial infarction.[2] Despite recent advancements in reperfusion therapy, no significant improvement has been achieved in the mortality rate during the late stages of the disease. This outcome is primarily attributed to myocardial ischemia-reperfusion injury (I/R) that occurs following the reopening of occluded coronary arteries, leading to various adverse reactions.[3] Reperfusion injury exacerbates myocardial cell damage, resulting in impaired contractile function, ultimately leading to arrhythmias and heart failure. Excessive production of ROS is one of the key factors contributing to myocardial cell injury. ROS trigger acute inflammation, leading to myocardial cell

Received: 31 October 2023
Accepted: 22 December 2023
Published: 12 January 2024

apoptosis. After myocardial cell death, the heart initiates a self-repair program, which ultimately leads to fibrotic scar formation, thereby negatively impacting cardiac function. Therefore, early antioxidant therapy followed by combination therapy is considered to ameliorate effectively myocardial ischemia-reperfusion injury.[4] Several antioxidant drugs that are appropriate for this therapeutic purpose have been developed, but their further research has been limited by low drug utilization rates and potential systemic side effects.[5,6] Gallic acid (GA, 3,4,5-trihydroxylbenzoic acid) is an important polyphenol compound present in various fruits, nuts, green tea and red wine with various biologic activities. It possesses potent antioxidant properties and additional research has validated its protective effects on the cardiovascular system.[7]

Nanomedicine shows great promise as a potential solution for oral drug delivery and nutritional supplementation.[8] It offers several advantages compared to traditional drugs, such as reducing systemic side effects, targeting delivery, and controlling release to improve drug usage.[9,10] A significant amount of research has focused on nanomedicines for managing myocardial ischemia-reperfusion injury. For instance, nanomedicines have been designed to regulate NOXs or ROS scavenging enzymes and modulate mitochondrial function, resulting in anti-inflammatory and antioxidant effects.[11,12] Bioactive glass has received considerable attention in both scientific and clinical settings due to its potential in tissue engineering and regenerative medicine. This material exhibits outstanding biocompatibility and beneficial biological activities, making it a versatile system for various applications, including tissue engineering, vascular regeneration, implant coatings, and drug delivery.[13] Depending on their glass network composition, bioactive glasses can be classified into silicate-derived, borosilicate/borate-derived, and phosphate-based variants. The unique structure of bioactive glass allows for the incorporation of various metallic ions like magnesium, zinc, strontium, and copper into the base composition. The in-situ release of these ions can produce specific therapeutic effects.[14] Additionally, mesoporous bioactive glass demonstrates excellent stability and high drug-loading capacity, making it an effective tool for targeted drug delivery.[15]

Recent studies on bioactive glass have shown promising potential for applications beyond traditional uses. While bioactive glass has been extensively explored in orthopedic implants and as a nanoplatform for targeted cancer therapy, efforts are now being directed towards its utilization in soft tissues, including cardiac tissue. The unique properties of bioactive glass, such as its biocompatibility and ability to promote tissue regeneration, make it an intriguing candidate for applications in cardiac therapy.[16,17] However, further research is required to fully understand and harness its potential in this specific context. By exploring the application of bioactive glass in cardiac tissue, innovative strategies for cardiovascular interventions and treatments may emerge, opening new avenues for regenerative medicine in the field of cardiology.

Based on the pathological process of myocardial ischaemia-reperfusion injury and the high plasticity of bioactive glass, we found that bioactive glass has great potential in the cardiovascular field and that there are very few studies on the application of bioactive glass in the cardiovascular field. Considering the potential compatibility issues arising from complex ion release in traditional bioactive glasses and their impact on the dynamic and highly specialized environment of the heart, we have changed the elements of the traditional mesoporous bioactive glass by adding magnesium at different concentrations, while not retaining calcium (Ca^{2+}). Furthermore, we introduced gallic acid as a model antioxidant drug loaded within the nanoparticles. The objective of this study was to achieve localized antioxidant effects through the controlled release of gallic acid from the loaded nanoparticles. In addition, we found that the magnesium-doped mesoporous bioactive glass induced phenotypic transformation of macrophages, reducing the secretion of inflammatory factors, while promoting the proliferation of vascular endothelial cells and angiogenesis. Ultimately, these beneficial activities improved cardiac function. Our findings suggest that magnesium-doped mesoporous bioactive glass holds promise as a novel therapeutic strategy for the treatment of myocardial ischemia-reperfusion injury.

Methods and Materials

Chemicals and Reagents

Tetraethyl orthosilicate (TEOS), 3-aminopropyltriethoxysilane (APTES), hexadecyl trimethyl ammonium bromide (CTAB), triethyl phosphate (TEP), ethyl acetate, and all organic chemicals were obtained from Sigma-Aldrich Trading Co., Ltd. cy7-NHS ester was obtained from Aladdin. Gallic acid was obtained from Sinopharm Chemical Reagent Co., Ltd. JC-1 solution, IL-1β ELISA Kit, IL-6 ELISA Kit, TNF-α ELISA Kit, ROS assay Kit, MDA assay Kit, SOD assay Kit, and GPx assay Kit were obtained from Beyotime Biotechnology Co., Ltd. 2% TTC solution was obtained from Solarbio Life Science Co., Ltd.

Synthesis of MgNPs

A mild sol–gel process was employed to synthesize magnesium doped mesoporous bioactive glasses nanospheres (MgNPs) of molar compositions 80Si/14P/6Mg (marked 6%MgNPs), 80Si/18P/2Mg (2%MgNPs), 80Si/20P/0Mg (NPs) from TEOS, and Magnesium nitrate hexahydrate ($Mg(NO_3)_2 \cdot 6H_2O$). As an example of synthesizing 6%MgNPs nanospheres, 0.7 g CTAB is used as the structure-directing agent, which is dissolved in 33 mL of deionized water to ensure full dissolution. Ten-milliliter ethyl acetate was added to the above solution as a pore-forming agent and stirred for 30 minutes. Then, 7mL 1mol/L $NH_3 \cdot H_2O$ was added to the solution from the previous step, and stir for 15 minutes to achieve the appropriate reaction environment. Then, 3.6mL TEOS, 0.51mL TEP, and 0.595g magnesium nitrate hexahydrate were added in every half hour interval.

Synthesis of MgNPs-cy7

The amine-functionalized silane APTES was employed to modify the MgNPs. In brief, 1 g MgNPs was introduced into 100 mL of toluene, after which 1 mL of APTES was added. The resulting mixture was refluxed at 80 °C for 20 hours, followed by centrifugation at 11,000 rpm for 15 minutes. Afterward, the sample was subjected to additional centrifugation and washed with absolute ethanol at 11,000 rpm for 15 minutes. Subsequently, it was subjected to lyophilization for 36 hours to obtain MgNPs-NH_2 powder. Next, we slowly added an appropriate amount of freshly prepared 10 mg/mL of cy7-NHS ester into 1 mL of MgNPs-NH_2, mixed gently, briefly centrifuged, and collected the sample at the bottom of the reaction tube to remove the free cy7-NHS and obtain MgNPs-cy7.

Characterization

TEM images and element mappings were obtained on JEM-200 (JEOL) microscope. SEM images were obtained on Sigma 300 and Gemini 300 (Zeiss). Nitrogen adsorption–desorption isotherm and pore-size distribution data were obtained on ASAP2460 (Micromeritics). XPS spectra were recorded by K-Alpha (Thermo Scientific). FTIR spectra were obtained on Nicolet iS 20 (Thermo Scientific). The gallic acid concentration in the solution was determined on UV-3600 i plus spectrometer (Shimadzu). CLSM images were obtained on FV3000 (Olympus). Flow cytometry was conducted on LSRFortessa X-20 (Becton Dickinson).

Drug Loading and in vitro Release

Gallic Acid Loading into MgNPs

The mixture of Gallic acid (GA) and PBS, at a concentration of 80 μg/mL, was combined with 50 mg of MgNPs and subjected to vibration for 24 hours. The supernatant was collected, and the precipitate was centrifuged, dried at 37°C to obtain GA loaded MgNPs (MgNPs/GA).

Drug Release in vitro

To assess the in vitro release of GA from MgNPs, the MgNPs/GA was submerged in 5 mL of PBS solution and incubated at 37 °C with shaking at 150 rpm for various time intervals ranging from 1 to 336 hours, with measurements taken at 1, 2, 4, 8, 12, 24, 36, 72, 168, 240, and 336 hours. At each interval, 2.5 mL of the release medium was collected, and an equal volume of fresh PBS was added back. The extracted medium was then analyzed by UV-Vis spectroscopy at a wavelength of 259 nm.

Assessment of Mg Ions Release

The samples were incubated in 20 mL PBS at 37°C. Next, the supernatant was collected for analysis and renewed with fresh PBS every time points. ICP-OES instrument (ICP-OES 720, Agilent, USA) was used to measure the Mg ion concentration released in all samples.

Biocompatibility of MgNPs

Cell Culture

Raw264.7, HL-1 and Human umbilical vein endothelial cells (HUVECs) were purchased from ATCC. HL-1 cells were cultured with DMEM supplemented with 10% fetal bovine serum (FBS) and 1% penicillin/streptomycin. HUVECs were cultured using the DMEM supplemented with 10% FBS and 1% penicillin/streptomycin. RAW264.7 were cultured with DMEM supplemented with 10% FBS and 1% penicillin/streptomycin. Cells were cultured in normoxic incubator (5% CO_2, 37°C).

Cell Cytotoxicity

The study employed HL-1 cells and HUVECs to examine cellular behavior. Cell viability was assessed using a cell counting kit-8. In brief, both cell types were seeded in 96-well plates at a density of 1×10^4 cells/well, followed by treatment with different groups. The cells were then incubated in DMEM supplemented with 10% FBS at standard conditions for 24 h and 72 h.

Blood Compatibility

To determine the blood compatibility of the nanoparticles, the thromboresistance was assessed using a previously published methodology. Briefly, an 80 μg/mL MgNPs solution in DPBS or DPBS mixed with 200 μL mouse blood and incubated at 37°C. The clotting of blood was initiated by adding 0.1 M $CaCl_2$. The supernatants were centrifuged at 0.5 and 2h and the absorbance of haemoglobin was measured at 540 nm.

JC-1 Staining

According to the protocol of the assay kit, prepare the following steps. In brief, take an appropriate amount of JC-1 solution and dilute it with ultrapure water at a ratio of 50 ul per 8 mL. After complete dissolution, add 2 mL staining buffer to obtain the JC-1 staining working solution. Next, add 1 mL of the JC-1 staining working solution per well in a six-well plate and incubate in a cell culture incubator for 30 minutes. After incubation, wash with buffer solution and observe under a fluorescence microscope.

Cell Uptake

The cellular uptake assay involved the incubation of cells seeded in 96-well plates with 40 μg/mL MgNPs-cy7 for a period of 2 hours. Following this, the cells were subjected to a series of procedures, which included washing, fixing, blocking, and staining with Phalloidin and DAPI. Thereafter, images were captured using a confocal microscope (Olympus FV3000). The uptake ratio was determined by calculating the percentage of cells that exhibited uptake of the nanoparticles.

RNA-Seq

Mouse hearts from the I/R model and MgNPs/GA treatment groups were taken, and total RNA was extracted from each sample and stored at 80°C. The cDNA libraries were created using the TruSeq Stranded mRNA Library Preparation Kit (Illumina, USA), following the manufacturer's procedure. The libraries were quality-controlled using an Agilent 2200 and Qubit 3.0, and after passing, sequenced using the Illumina HiSeq X ten platform. We performed differential analysis using DESeq2 v1.40.2. Differentially expressed genes (DEGs) were identified by setting the log2FoldChange threshold to 0.5 and adjusting the p-value (padj) to be less than 0.05 for differential analysis of the I/R vs MgNPs/GA groups. Prior to GSEA analysis, we ranked the genes with significant P values. This ranking was performed based on log2FoldChange values to identify genes with significant changes in expression. Subsequently, we performed genomic enrichment analysis using genomic data obtained from the Molecular Signature Database (MSigDB) and using ClusterProfiler V4.8.2 R software.

In vitro Assessment of Angiogenesis

HUVECs Migration

To initiate the migration process in HUVECs, a 6-well plate was used to culture the cells until a monolayer was formed at a confluency level of 90–100%. Subsequently, the monolayer was disrupted by scraping a 200 μL pipet tip across its surface, then washed and replenished with serum-free medium containing different treatment groups. After a 6-hour incubation period, images of the scratch were captured using an optical microscope. The distance between the two edges of the scratch was measured using Image J software.

HUVECs Tube Formation

The experiment involved seeding HUVECs into a matrigel at a density of 5×10^5 cells/mL. The cells were cultured under standard conditions and treated with serum-free medium containing either treatment (10 mg/mL) or no supplement.

Macrophage Polarization Analysis

CD206/iNOS Immunofluorescence Staining

Cells were incubated at room temperature in 4% paraformaldehyde (dissolved in PBS, pH 7.4) for 10 minutes. Cells were washed three times with PBS. Samples were incubated in PBS (containing 0.1% Triton X-100) for 10 minutes. Cells were washed three times with PBS, each wash lasting for 5 minutes. Cells were incubated with blocking solution for 30 minutes. At room temperature, cells were co-incubated overnight with diluted antibodies CD206 (Abcam, 1ug/mL, rabbit) and iNOS (Abcam, 1ug/mL, mouse) at 4°C. The solution was poured out, and cells were washed three times with PBS, each wash lasting for 5 minutes. At room temperature, cells were incubated for 1 hour with Goat Anti-Rabbit IgG H&L (Abcam, cy3, 1:1000) and Goat Anti-Mouse IgG (Abcam, FITC, 1:1000) in the dark. The secondary antibody solution was poured out, and cells were washed three times with PBS in the dark, each wash lasting for 5 minutes.

Macrophage Polarization-Related Gene mRNA Expression

Cells were collected, and total RNA was extracted using the Simply P Total RNA Extraction Kit (BioFlux, China). After reverse transcription, real-time PCR was performed to detect the expression of the four main genes ARG1, CD163, TNF-α and IL-8 by RT-qPCR using β-actin as the internal reference gene. The primer sequences used are shown in Table 1.

Inflammatory Factors

Macrophages were cultured in 6-well dishes, with the addition of each set of samples occurring once the cells reached full confluence. After 24 hours, the supernatant from the macrophages was collected, and the levels of IL-1β, IL-6, and TNF-α were measured utilizing ELISA kits according to the provided protocol.

Reactive Oxygen Species Scavenging

H/R Model

HL-1 cells and RAW264.7 were exposed to in vitro hypoxia utilizing an oxygen control system (Changjin Technology, China), which had the capability to establish hypoxic conditions using a blend of 95% nitrogen and 5% CO_2. The HL-1 cells were subjected to treatment by culturing them in a serum- and glucose-free medium under hypoxic conditions (<1% O_2) for 4 hours. Subsequently, upon restoring normal gas conditions, the cells were cultured either in regular medium or in medium containing samples sourced from distinct groups for 3 days. Finally, the cell viability and apoptosis were assessed.

Intracellular ROS Levels

Intracellular levels of ROS were assessed using 2',7'-dichlorodihydrofluorescein diacetate (DCF-DA), a fluorescent probe. Specifically, cells were incubated with 10 μM DCF-DA. After incubation at 37 °C for 20 minutes, fluorescence of DCF (the deacetylated product of DCF-DA) was visualized using confocal microscopy, or cell samples were collected, and fluorescence intensity was measured using flow cytometry after incubation with 10 μM DCF-DA.

Table 1 Primer Used in This Study

Gene and Primer Direction		Sequence (5' to 3')
Mouse ARG1	Forward	CTCCAAGCCAAAGTCCTTAGAG
	Reverse	AGGAGCTGTCATTAGGGACATC
Mouse CD163	Forward	ATGCTTCCATCCAGTGCCTC
	Reverse	CACAAACCAAGAGTGCCGTG
Mouse TNF-α	Forward	CGGGCAGGTCTACTTTGGAG
	Reverse	ACCCTGAGCCATAATCCCCT
Mouse IL-8	Forward	GTCCTTAACCTAGGCATCTTCG
	Reverse	TCTGTTGCAGTAAATGGTCTCG
Mouse β-actin	Forward	CACTGTCGAGTCGCGTCC
	Reverse	TCATCCATGGCGAACTGGTG

Abbreviations: ARG1, Arginase-1; TNF-α, tumor necrosis factor-α; IL-8, Interleukin-8; β-actin, Beta-actin.

Enzyme Activity Analysis

The levels of MDA, SOD, and GPx activity were assessed to evaluate the extent of oxidative stress. Briefly, cell samples from each group (Control, H/R, MgNPs+H/R and MgNPs/GA+H/R) were collected and centrifuged at 4000 g for 10 minutes to obtain the cell lysates supernatant. The levels of MDA and SOD, as well as the GPx activity in the supernatant, were quantified using commercially available assay kits.

Animals

Six-week-old C57BL/6 mice (25±2 g) were purchased from Shanghai JieSiJie Laboratory Animal Co., Ltd. The Institutional Animal Care and Use Committee at The First Affiliated Hospital of Nanchang University approved the proposed protocols (Approval Code: CDYFY-IACUC-202209QR009). The Laboratory Animal Guidelines for Ethical Review of Animal Welfare (GB/T 35892–2018) was followed to ensure the welfare of the laboratory animals. After surgery, the mice were placed in a normal environment for routine rearing and fed food and water regularly. The mice were euthanised before experiments were performed at various time points.

I/R Model

The mouse was anaesthetized with 2% isoflurane and fixed in the supine position on the operating table. An incision with an approximate length of 1 cm was made between the 3rd and 4th ribs on the left side of the sternum along the edge of the pectoralis major muscle, and the subcutaneous tissue; the pectoralis major and serratus anterior muscles were bluntly separated. The left anterior descending branch of the coronary artery was ligated with a 6–0 wire 2 mm below the left auricle. The ligature was tied in a live knot, with the proximal end cut short and the distal end left 3–4 cm outside the chest cavity. After ligation, the ventricular wall below the ligature turns dark red and the heart was slowly pushed into the thoracic cavity. Further, the heart was slowly pushed into the thoracic cavity. The thoracic cavity was squeezed out, and the chest wall incision was tightened with a purse-string knot. Then, the thoracic cavity was closed. After 60 min of ischemia, the ligature was slowly pulled out to restore myocardial blood supply. Mouse body weights were recorded at each time point and mice were observed daily for survival.

Myocardial Multi-Regional Injection

The mice were randomly divided into five groups: I/R, GA+I/R (300 μg/kg), NPs+I/R (80 μg/mL), MgNPs+I/R (80 μg/mL), and MgNPs/GA+I/R (80 μg/mL). Injections were made on day 2 postoperatively. During the administration of anesthesia, the heart was exposed by means of an identical left thoracotomy procedure. A total volume of 75 μL of the treatment solution in saline or pure saline was injected into the regions encompassing the infarction, specifically the apical, proximal, lateral, and septal walls, along with the core of the infarction itself (5 injections, with each region receiving 15 μL). Multi-region injection allows for more even distribution within the myocardium.

Cardiac Function Assessment

Assessment of cardiac function using echocardiography was performed at day zero and 28 days post-surgery, using the Vevo 2100 imaging system (VisualSonics Inc., Toronto, Canada). The cardiac function parameters measured were left ventricular ejection fraction (LVEF), left ventricular fractional shortening (LVFS), left ventricular end-diastolic volume (LVEDV), and left ventricular end-systolic volume (LVESV).

TTC Staining

Anesthetized mice were euthanized, and the chest was opened to remove the heart, which was preserved on dry ice. Upon freezing fixation of the heart, it was placed in a slicer, and consecutive 1 mm-thick sections were cut starting from the apex, yielding a total number of five sections. Subsequently, the sections were incubated in a 2% TTC staining solution at 37 °C for 8 minutes. After staining, the sections were washed with PBS to remove excess staining solution and then stored in 4% paraformaldehyde for further use.

Tissue Immunofluorescence Staining

Fresh cardiac tissue from the ischemic area was collected for frozen sections at 6 hours post-surgery, followed by CM-H2DCFDA (Thermo Fisher, 1:150) and TUNEL staining (Beyotime Biotechnology). Fresh heart tissue was collected at day 14 post-surgery, fixed with 4% paraformaldehyde, and embedded in paraffin. Immunofluorescence staining for CD31 (Abcam, 1:200), CD206

(Proteintech Group, 1:1000), CD68 (Boster Bio, 1:200), Ki67 (Abcam, 1:2000), and PGC-1α (Proteintech Group, 1:200) were performed. To evaluate the early tissue ROS levels during reperfusion, samples were collected at 6 hours post-surgery and stained with CM-H2DCFDA. Additional samples were collected for TUNEL staining to assess myocardial cell survival. Next, to evaluate angiogenesis during cardiac repair, tissue samples were collected at day 14 post-surgery and subjected to CD31 immunofluorescence staining. Additionally, to assess the levels of M2 macrophages in the ischemic site, tissue samples were collected at day 14 post-surgery, which was then subjected to immunofluorescence staining for CD206 and CD68.

Statistical Analysis

The data were presented as mean ± standard deviation. One-way analysis of variance (ANOVA) with the Student-Newman-Keuls method was performed for the statistical analysis of intergroup measurement variability. A p-value of less than 0.05 was considered statistically significant.

Results

Characterization of MgNPs

In this study, MgNPs were successfully synthesized using sol-gel technique with CTAB as the template (Scheme 1). The surface morphology and physicochemical properties of the nanoparticles after the incorporation of Mg into the NPs

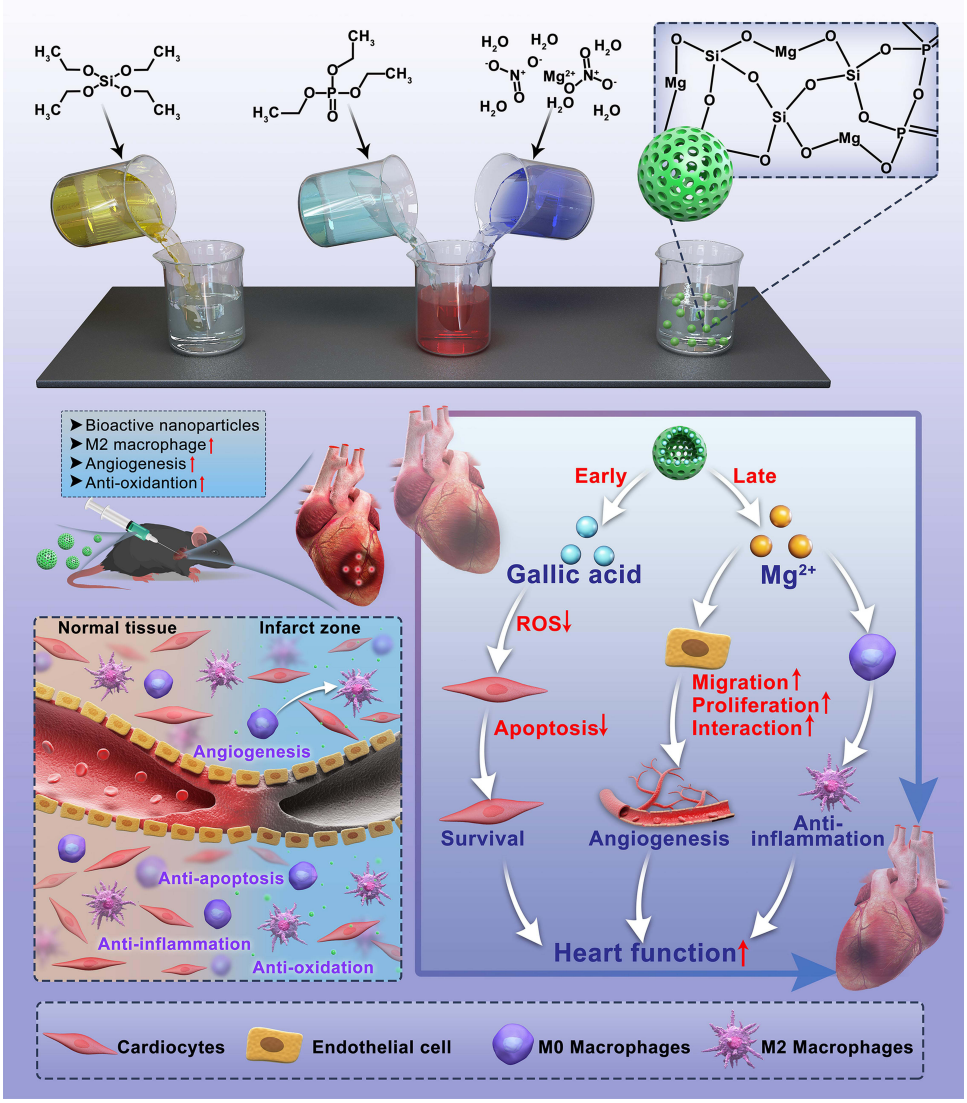

Scheme 1 Scheme of the preparation and evaluation of the MgNPs/GA.

structure were observed through scanning electron microscopy (SEM), transmission electron microscopy (TEM), Brunauer–Emmett–Teller (BET) analysis, X-ray photoelectron spectroscopy (XPS), and Fourier-transform infrared spectroscopy (FTIR). The results revealed that the synthesized MgNPs had a spherical morphology with mesoporous structures on the surface (Figure 1A and B). The incorporation of Mg did not significantly affect the particle size, which remained at an average of approximately 146 nm (Figure 1H).

All BET isotherms showed a typical-type IV adsorption–desorption curve with hysteresis loops, indicating a mesoporous structure and a narrower size distribution of 2%MgNPs and 6%MgNPs (Figure 1C–E). The specific surface area of 2% MgNPs was the highest, measuring 744.18 ± 12.78 m²/g, surpassing that of 6% MgNPs (716.10 ± 12.94 m²/g) and NPs (713.32 ± 12.64 m²/g). The mesopore volumes of the magnesium-doped mesoporous bioactive glass were 0.87, 0.96, and 0.83 cm³/g, respectively. The magnesium-doped mesoporous bioactive glass maintained a high specific surface area, implying a better contact between nanoparticles and the medium, which is favorable for the degradation of nanoparticles. X-ray photoelectron spectroscopy (XPS) spectra not only detected the peaks for C1s, O1s, Si2p, and P2p, but also identified the peak for Mg1s (Figure 1G).

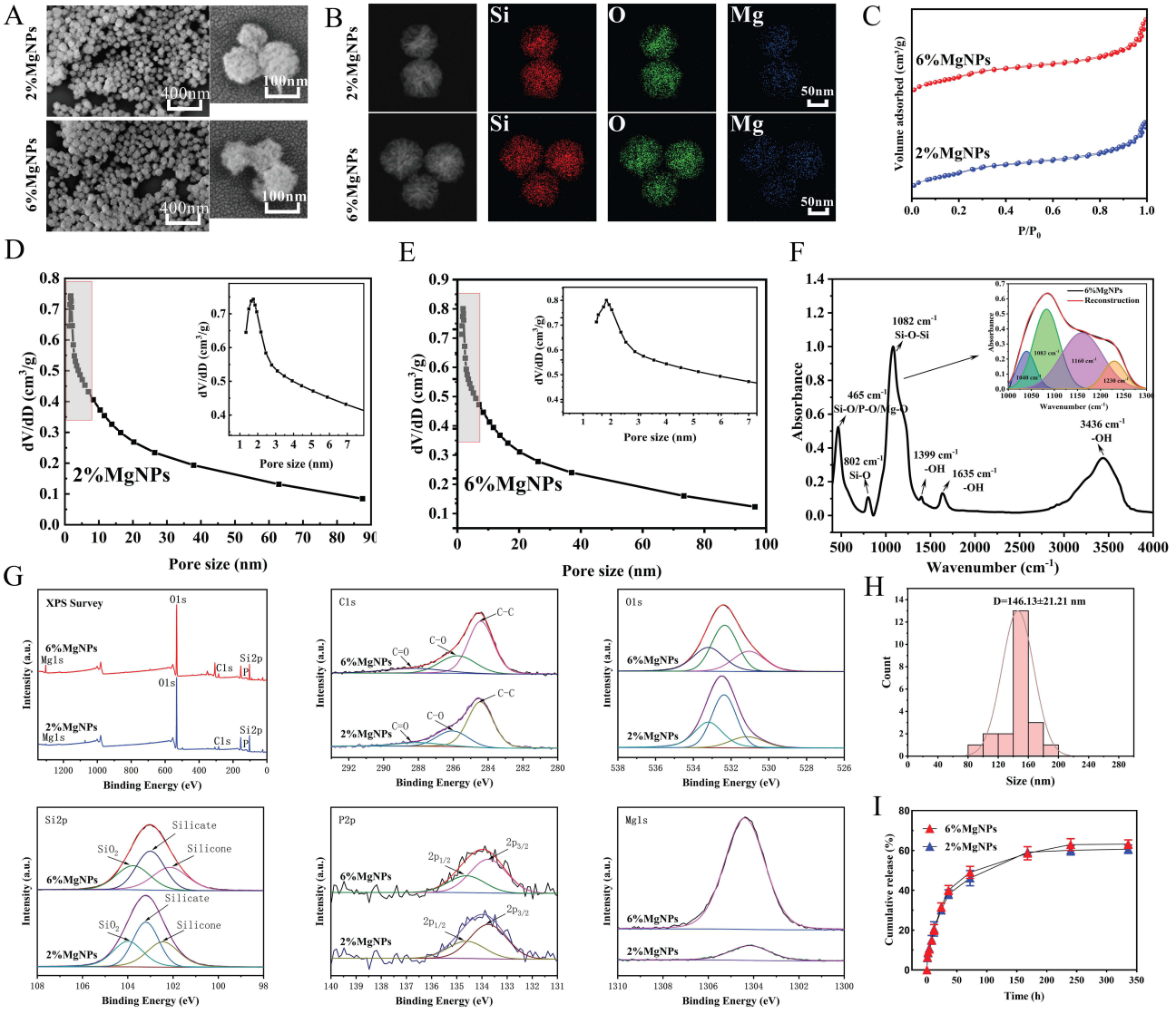

Figure 1 Characterisation of MgNPs at different concentrations. (**A**) Scanning electron microscope images of MgNPs at different concentrations, scale bar: 50nm. (**B**) TEM-EDS images at different concentrations, scale bar: 50nm. (**C–E**) N_2 adsorption-desorption analysis and pore size distributions of 2%MgNPs and 6%MgNPs. (**F**) FTIR spectra of 6%MgNPs. (**G**) XPS survey scan and peak fitting of MgNPs at different concentrations. (**H**) Particle size distribution. (**I**) Gallic acid release profile of 2%MgNPs and 6% MgNPs in vitro. Results are presented as mean ± SD (N = 3).

In the infrared spectra (Figure 1F), the absorption peaks at 3436 cm^{-1}, 1635 cm^{-1}, and 1399 cm^{-1} primarily arise from the stretching and bending vibrations of –OH groups, indicating the presence of trace amounts of bound water/adsorbed water in the samples. A broad and intense absorption band appeared at 1082 cm^{-1}, which was attributed mainly to the asymmetrical stretching vibrations of Si-O-Si bonds (from the tetrahedral structure of silicon) and stretching vibrations of O-Si-O bonds (within the tetrahedral structure of silicon).[18] An apparent shoulder peak was observed on the right side of this absorption peak, and the fitting results for this region also revealed the presence of four or more sub-peaks, suggesting a significant shift in the Si-O absorption peak. This could potentially be due to the inclusion of P-O stretching vibration modes and the potential incorporation of elements such as Mg and P into the interlayer structure of Si-O.[18,19] The absorption peak observed at 802 cm^{-1} was attributed to the symmetric stretching vibration mode of Si-O bonds in silicon dioxide molecules. The absorption peak at 465 cm^{-1} was primarily associated with the bending vibration modes of Si-O and P-O bonds, possibly indicating the presence of structures involving Mg-O, among others.

Drug Release of MgNPs

The concentration of GA before and after loading was measured using a UV spectrophotometer. The maximum UV absorption peak was observed at 259 nm, indicating the successful loading of GA into MgNPs. The encapsulation efficiency and drug loading efficiency of 6% MgNPs were determined to be 16.22 ± 0.47% and 13.53 ± 0.28%, respectively, while those of 2% MgNPs were found to be 18.07 ± 0.36% and 14.26 ± 0.21%, respectively. The cumulative-release profiles of 6% MgNPs and 2% MgNPs are displayed in Figure 1I. GA was rapidly released within 36 hours, followed by a stable-release state; complete release achieved at 168 hours. Ultimately, the cumulative release rates of 6% MgNPs and 2% MgNPs were approximately 63.15% and 60.68%, respectively. The release of Mg^{2+} was stable over the 14-day period, and there was no sudden release. The cumulative releases of the 2% MgNPs and the 6% MgNPs over the 14-day period were about 1.388±0.091mg/L and 3.884±0.200 mg/L (Figure S1). The MgNPs and MgNPs/GA used in the following studies were 6% MgNPs.

Biocompatibility of MgNPs

Considering biological safety, it was necessary to evaluate the cytotoxicity of nanoparticles (NPs) for cellular applications.[20] NPs, MgNPs, and MgNPs/GA were co-cultured with HL-1 and HUVECs at various concentrations (0–200 μg/mL) for 24 and 72 hours (Figure 2A). MgNPs and MgNPs/GA showed obvious proliferation effects when co-cultured with HUVECs for 24 and 72 hours. Although NPs did not exert significant proliferation effects, they showed no apparent cytotoxicity within a concentration range of up to 100 μg/mL. When co-cultured with HL-1 for 24 and 72 hours, NPs, MgNPs, and MgNPs/GA exhibited no significant cytotoxicity within a concentration range of up to 100 μg/mL. However, cell viability significantly decreased after the concentration exceeded 100 μg/mL. Additionally, live/dead staining and cell morphology were further assessed to verify the impact of the nanoparticles on cells. When co-cultured with cells at a concentration of 80 μg/mL, NPs, MgNPs, and MgNPs/GA did not induce cell death, and HL-1 cell morphology remained normal. The results demonstrated that the tested samples did not cause cell deformation or loss of cellular viability (Figure 2B and C). JC-1 staining showed that after co-culturing with cells for 24 hours, the mitochondrial membrane potential remained unchanged, indicating normal mitochondrial function and the absence of early apoptosis (Figure 2D). To investigate the internalization of MgNPs/GA nanoparticles by HL-1 cells, Cy7-labeled MgNPs/GA nanoparticles were used for co-culturing, confirming the uptake of MgNPs/GA nanoparticles (Figure 2E). Moreover, transmission electron microscopy revealed substantial adsorption of nanoparticles on the cell surface (Figure 2F). To facilitate our subsequent in vivo experiments, it was important to confirm if the tested samples would lead to hemolysis reactions.[21] Across various concentrations, none of the tested samples showed signs of hemolysis (Figure 2G). In summary, the NPs, MgNPs, and MgNPs/GA prepared in this study exhibited no cytotoxicity to HL-1 cells within a specific concentration range. Furthermore, the released ions from the samples did not cause mitochondrial damage.

RNA-Seq Analysis

Differential gene expression analysis revealed distinct transcriptional landscapes between the I/R group and the MgNPs/GA treated group. We identified 132 downregulated genes and 33 upregulated genes following MgNPs/GA treatment (Figure 3A). In the heatmap, inflammation-related genes were prominently highlighted, demonstrating the downregulation of inflammation-

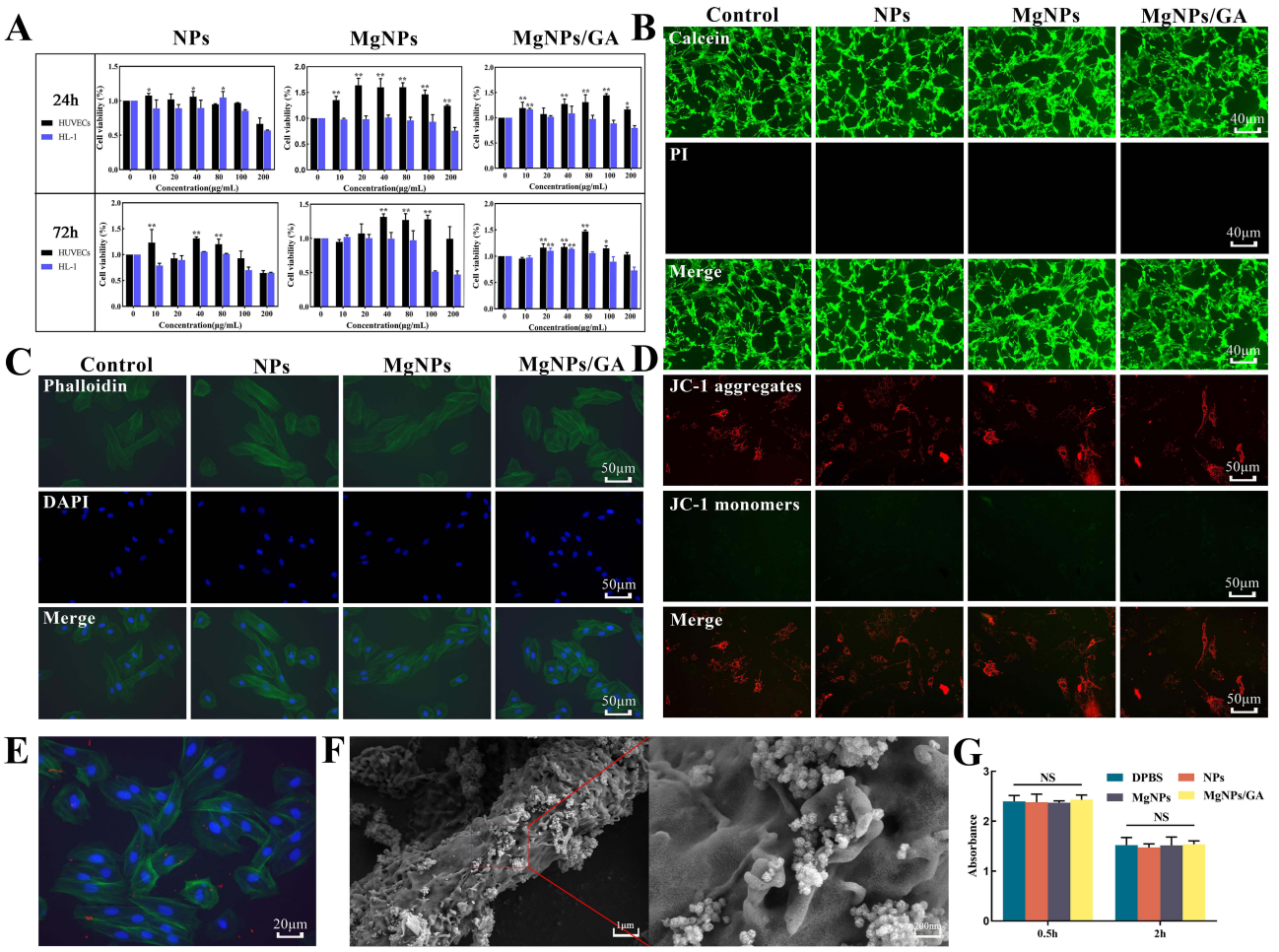

Figure 2 Biocompatibility and haemocompatibility of MgNPs/GA. (**A**) Cell viability at 24h and 72h after treatment of HL-1 and HUVECs in different samples. (**B**) Live-dead staining of samples from each group after treatment with HL-1, scale bar:40μm. (**C**) CLSM images of the morphology of HL-1 after 24 h treatment with each group, scale bar: 50μm. (**D**) fluorescence microscope images of the JC-1 staining after 24 h treatment with each group, scale bar: 50μm. (**E**) Uptake of MgNPs by HL-1, scale bar: 20μm. (**F**) Bio-Scanning Electron Microscope Images of HL-1 after 24 h treatment with MgNPs. (**G**) Thromboresistance test of each group, Results are presented as mean ± SD (N = 3), NS = not significant ($P > 0.05$), *$P < 0.05$, **$P < 0.01$.

related genes in the MgNPs/GA-treated group (Figure 3B). Furthermore, based on gene set enrichment analysis, we identified a downregulation trend in transcriptional features related to signal transduction pathways, specifically inflammation response and immune response, following MgNPs/GA treatment (Figure 3C and D).

Reactive Oxygen Species Scavenging

Acute excessive production of ROS induces oxidative stress, leading to significant cellular dysfunction, cell death, and even organ dysfunction.[22] In this study, gallic acid was loaded into nanoparticles as a model drug, which gradually degraded, allowing for local sustained release of gallic acid. The MgNPs/GA group had a significantly higher rate of reactive oxygen species clearance than the control, H/R, and MgNPs groups (Figure 4A, B, D and E). Although the results showed that not all reactive oxygen species were cleared, this is attributed to incomplete drug release. As the drug concentration increases, the rate of reactive oxygen species clearance would further improve. Once reactive oxygen species are promptly cleared, the cell survival rate of myocardial cells significantly increases (Figure 4C and F). Consistent with these results, treatment with MgNPs/GA significantly inhibited the excessive production of typical oxidative mediators such as malondialdehyde (MDA) induced by hypoxia/reoxygenation (Figure 4G). In contrast, the decline in hypoxia/reoxygenation-mediated glutathione peroxidase (GPx) and superoxide dismutase (SOD), both typical antioxidant proteins, was significantly reversed after incubation with MgNPs/GA (Figure 4H and I). Therefore, MgNPs/GA effectively reduces intracellular ROS generation, suppresses oxidative stress, and improves the survival rate of myocardial cells.

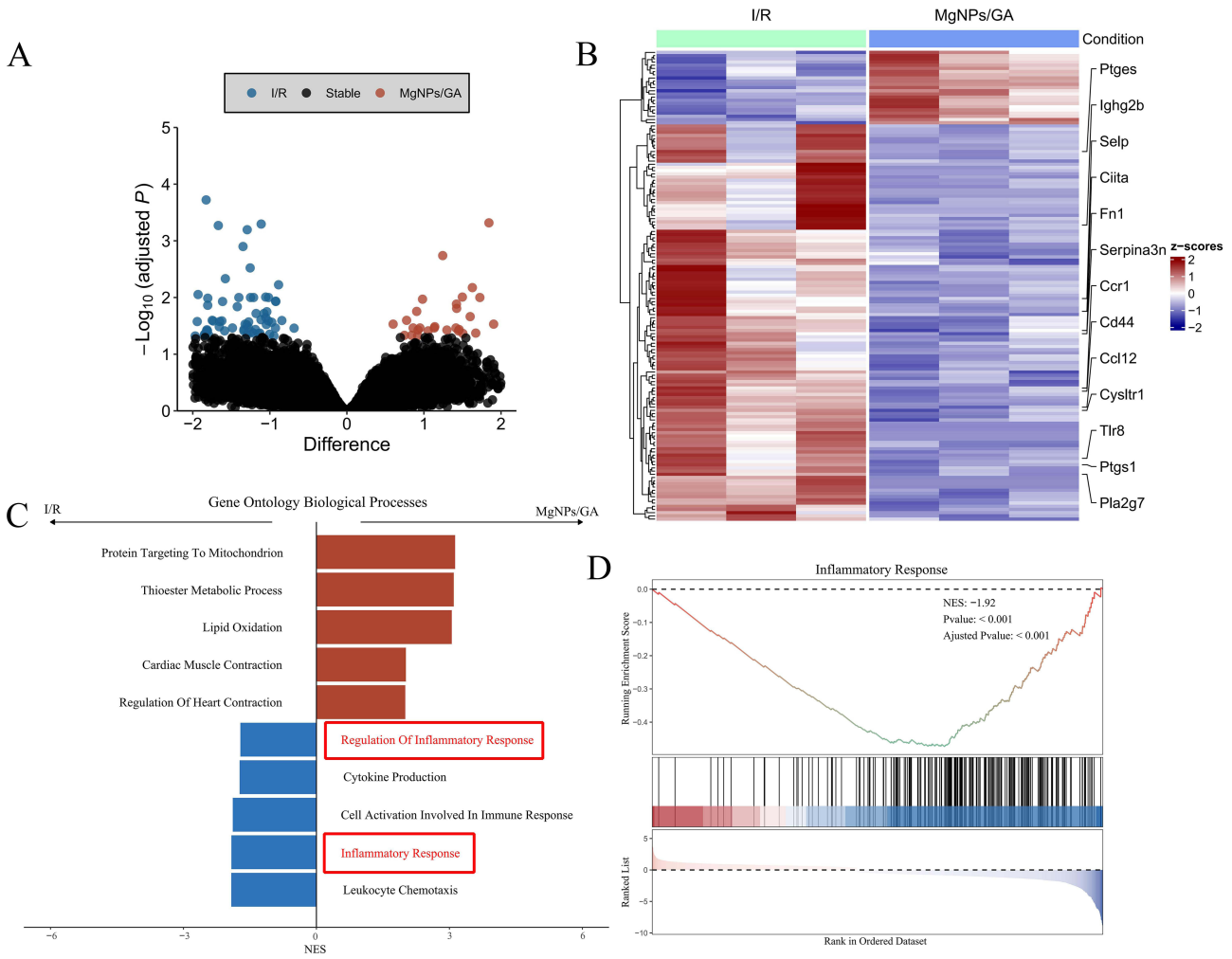

Figure 3 Association of MgNPs/GA Treatment with Inflammatory Signaling Pathways. (**A**) Displays the differential gene expression (log2 FoldChange) and q-values (-log10 adjusted P-values) from DESeq2 differential analysis between the I/R group (N = 3) and the MgNPs/GA group (N = 3). Each point represents a gene, with significantly differentially expressed genes (q < 0.05) color-coded. (**B**) Heatmap illustrates the expression of inflammation-related genes in I/R mice treated with MgNPs/GA. Inflammation-related genes were obtained from the Molecular Signatures Database (MSigDB) gene sets. Gene set enrichment analysis (GSEA) results show (**C**) pathway-normalized enrichment scores based on significance levels and (**D**) corresponding enrichment plots for the inflammation response signaling pathway.
Abbreviations: GSEA, gene set enrichment analysis; FDR, false discovery rate; NES, normalized enrichment score.

In vitro Angiogenesis

We conducted a series of functional assays to evaluate the effects of NPs, MgNPs, and MgNPs/GA on HUVECs. Specifically, we focused on two key aspects: cell migration and tubule formation. Cell migration is a fundamental process under various physiological and pathological conditions, including angiogenesis. As can be seen in Figure 5A and B, compared to the Control, GA, and NPs groups, both MgNPs and MgNPs/GA significantly enhanced the migration of HUVECs, indicating the expected effect of Mg^{2+}. In addition to cell migration, we also assessed the effects of NPs, MgNPs, and MgNPs/GA on tubule formation, a critical step in the development of vascular networks. Our results demonstrated that HUVECs treated with MgNPs and MgNPs/GA exhibited an increased ability to form organized and interconnected tubular structures in the tubule formation assay, indicating their effective angiogenic properties (Figure 5C–E).

Macrophage Polarization Analysis

To verify whether the release of Mg^{2+} from nanoparticles could induce macrophage phenotype transformation, various samples (Blank, H/R, GA+H/R, NPs+H/R, MgNPs+H/R, and MgNPs/GA+H/R) were co-cultured with macrophages for 24 hours, followed by observation using CD206/iNOS immunofluorescence staining (Figure 6A and B). In the H/R, GA +H/R, and NPs+H/R groups, iNOS expression was significantly upregulated, whereas that of CD206 was downregulated.

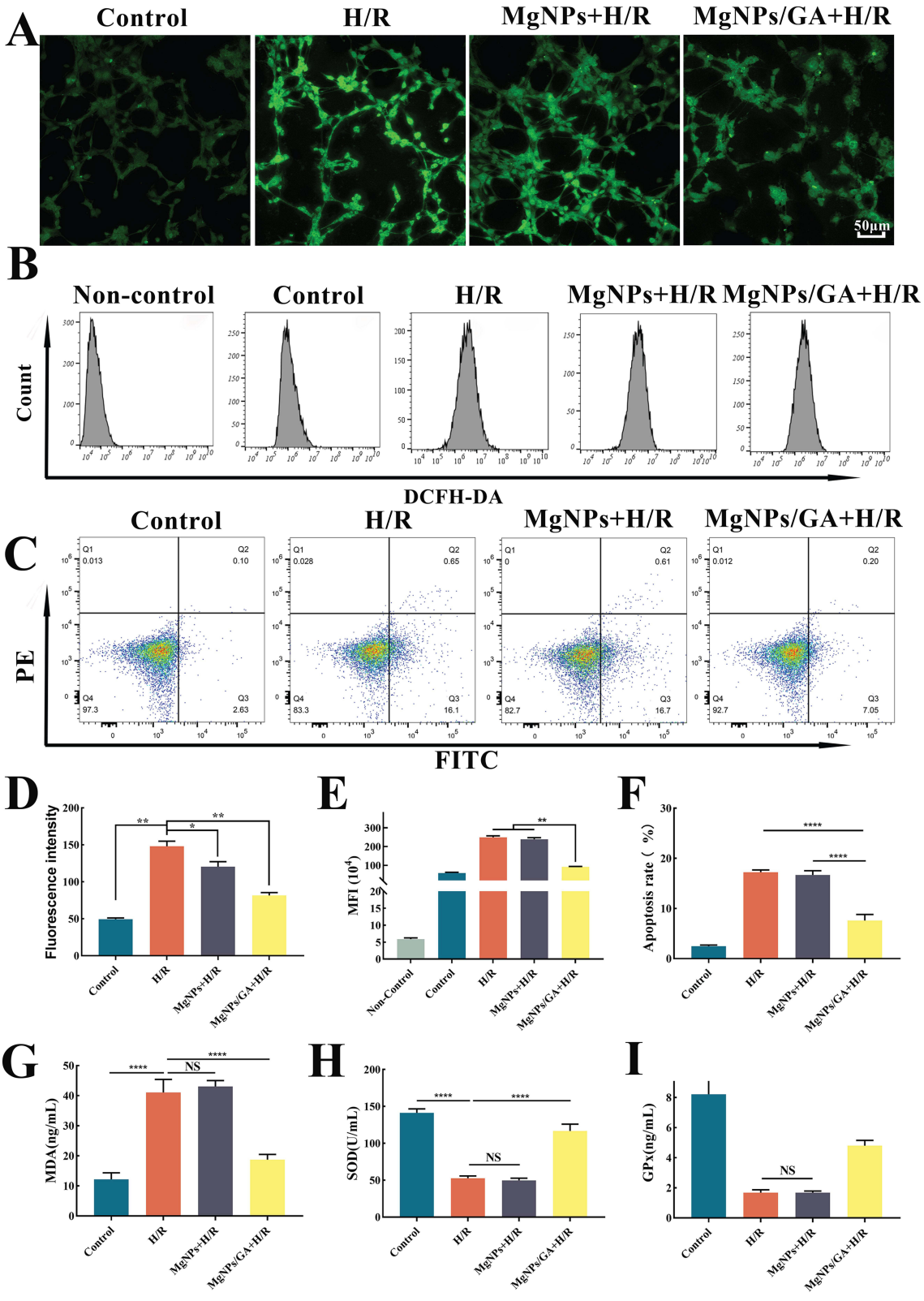

Figure 4 In vitro antioxidant effects of MgNPs/GA. (**A**) Fluorescent probe DCFH-DA staining images of HL-1 after 24 h treatment with each groups, scale bar: 50μm. (**B**) Detection of intracellular DCFH-DA fluorescent probe by flow cytometry. (**C**) Percentage of apoptosis detected by flow cytometry. (**D**) Quantification of DCFH-DA staining with fluorescent probes. (**E**) Quantification of the mean fluorescence intensity after flow cytometry. (**F**) Quantification of the percentage of HL-1 apoptosis after flow cytometry detection. (**G**–**I**) MDA, SOD and GPx levels were measured by ELISA kits. Results are presented as mean ± SD (N = 3), NS = not significant ($P > 0.05$), *$P < 0.05$, **$P < 0.01$, ****$P < 0.001$.

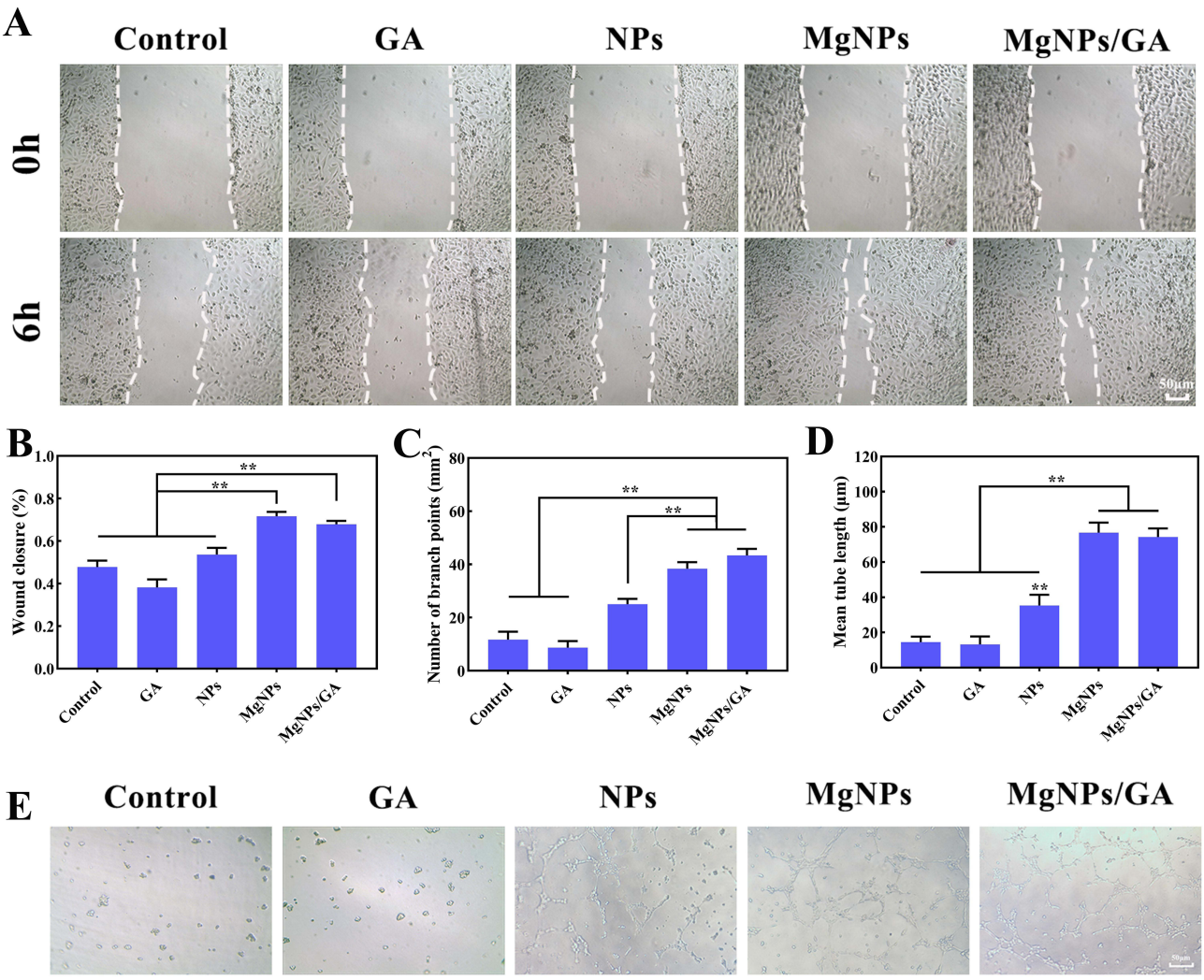

Figure 5 In vitro assessment of angiogenesis. (**A** and **B**) Cell migration assay and quantitative analysis, scale bar: 50μm. (**C**) Branch point quantitative analysis of tube formation. (**D**) Mean tube length quantitative analysis of tube formation. (**E**) Images of tube formation of HUVECs after 12 h treatment with each groups, scale bar: 50μm. Results are presented as mean ± SD (N = 3), **P < 0.01.

Conversely, the treatment with MgNPs and MgNPs/GA led to the upregulation of CD206 expression and downregulation of iNOS expression. Additionally, the expression of M1-related genes TNF-α and IL-8, as well as M2-related genes ARG1 and CD163, was assessed after the H/R model. As can be observed in Figure 6C, the treatment with MgNPs and MgNPs/GA significantly upregulated the expression of M2-related genes ARG1 and CD163, whereas the expression of M1-related genes TNF-α and IL-8 was upregulated in the H/R, GA+H/R, and NPs+H/R groups, showing the reverse trend for ARG1 and CD163 expression. Furthermore, the release of inflammatory factors was measured, and compared to the Blank group, the H/R, GA+H/R, and NPs+H/R groups showed a significant increase in the release of TNF-α, IL-1β, and IL-6, while the release of inflammatory factors was significantly reduced in the MgNPs+H/R and MgNPs/GA+H/R groups (Figure 6D–F). Our results indicate that Mg^{2+} promotes M2 macrophage polarization and reduces the secretion of inflammatory cytokines.

Angiogenesis, Oxidative Stress, Inflammation, and Cardiac Function Following Myocardial Ischemia-Reperfusion

Reperfusion injury exacerbates widespread cell death in the heart. To determine whether MgNPs/GA can effectively scavenge reactive oxygen species, promote M2 macrophage polarization, reduce the release of inflammatory factors, increase cardiomyocyte survival, and enhance tissue vascular regeneration to improve heart function, we performed multi-point injections of MgNPs/

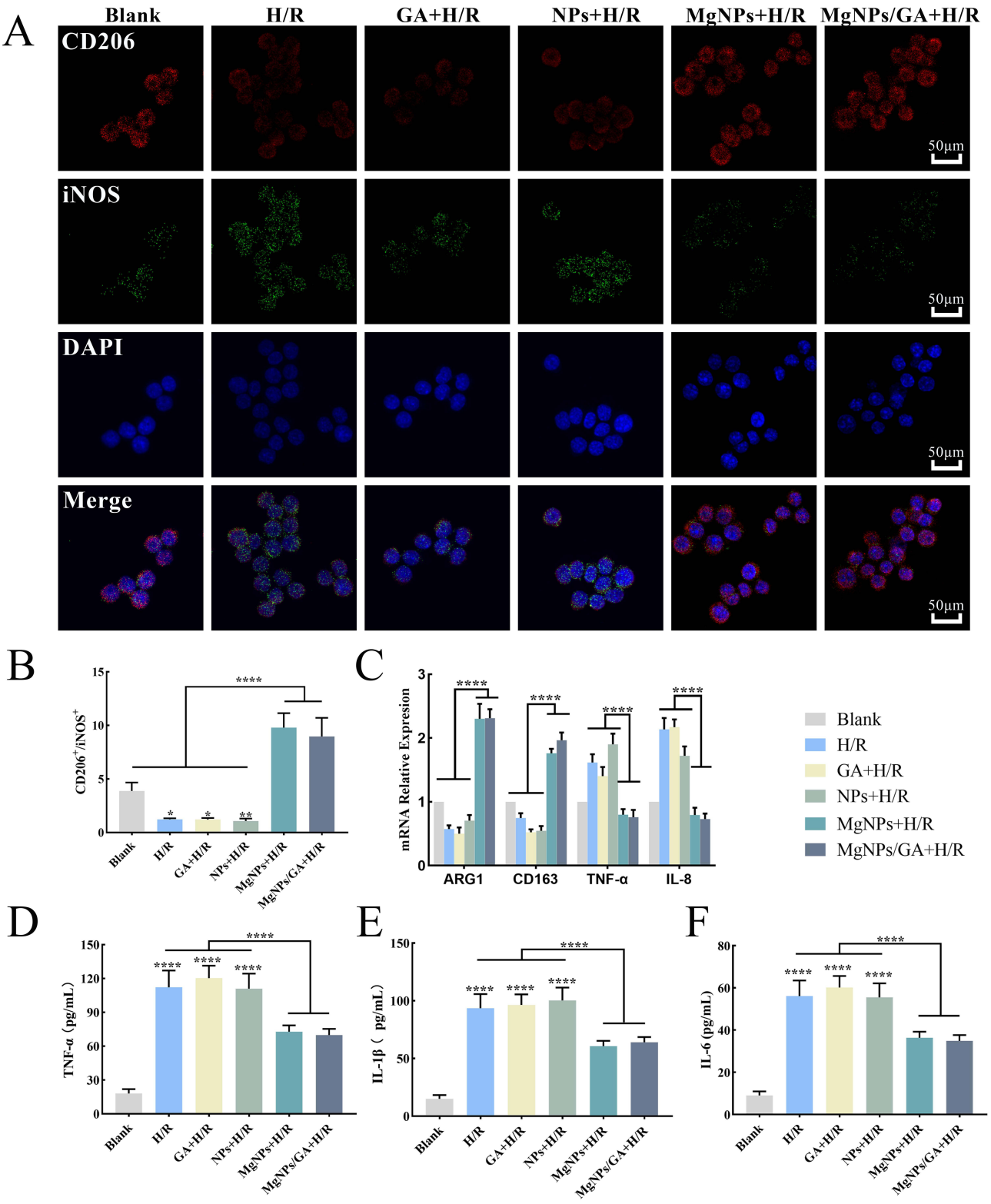

Figure 6 Anti-inflammatory effects of MgNPs/GA in vitro. (**A** and **B**) CD206/iNOS immunofluorescence images and quantitative analysis of fluorescence intensity, scale bar: 50μm. (**C**) PCR analysis of the expression of M1-related genes TNF-α, IL-8 and M2-related genes ARG1 and CD163. (**D**–**F**) Detection of inflammatory factors TNF-α, IL-1β and IL-6. Results are presented as mean ± SD (N = 3), *P < 0.05, **P < 0.01, ****P < 0.001.

GA during coronary artery ligation and conducted pathological examinations at 24 hours and 14 days after reperfusion (Figure 7A). The I/R, GA, and NPs groups were set as control groups. Excessive production of reactive oxygen species in the early stages of reperfusion injury leads to myocardial cell damage and death. Therefore, we examined whether GA released from MgNPs/GA could stably release and exert antioxidant biological effects at 24 hours after reperfusion. As visible in Figure 7B and D, the I/R, NPs, and MgNPs groups had a substantial accumulation of reactive oxygen species in the infarct area, whereas the GA and MgNPs/GA groups showed a significant reduction in reactive oxygen species in the infarct area, indicating the antioxidative effect exerted by GA released from the nanoparticles. With the scavenging of ROS, the cardiomyocytes were largely prevented from further damage, ultimately leading to increased survival of the cardiomyocytes (Figure S2). Sustained angiogenesis and anti-inflammatory effects are beneficial for cardiac repair and improved heart function.[23–25] Hence, 14 days after nanoparticle injection, we further investigated angiogenesis and the inflammatory response in the infarct area. In the stage of cardiac repair, both the MgNPs and MgNPs/GA groups exhibited a significantly higher number of blood vessels compared to the I/R, GA, and NPs groups (Figure 7C and E). Moreover, the number of M2 macrophages in the infarct area was significantly higher in the MgNPs and MgNPs/GA groups compared to the I/R, GA, and NPs groups (Figure 7F–H). MgNPs/GA also enhanced mitochondrial biogenesis in cardiomyocytes as peroxisome proliferator-activated receptor co-activator 1-alpha (PGC-1α)-positive cardiomyocyte densities were significantly increased (Figure S3). The highest PGC-1α-positive cell densities and the highest densities of Ki67-positive cells were observed in the MgNPs/GA group (Figure S4). These findings suggest that both GA and Mg^{2+} have their respective roles, and although GA is not involved in the subsequent repair phase, its scavenging of reactive oxygen species at an early stage provides a prerequisite for the role of Mg^{2+} in the subsequent cardiac repair phase. Our study

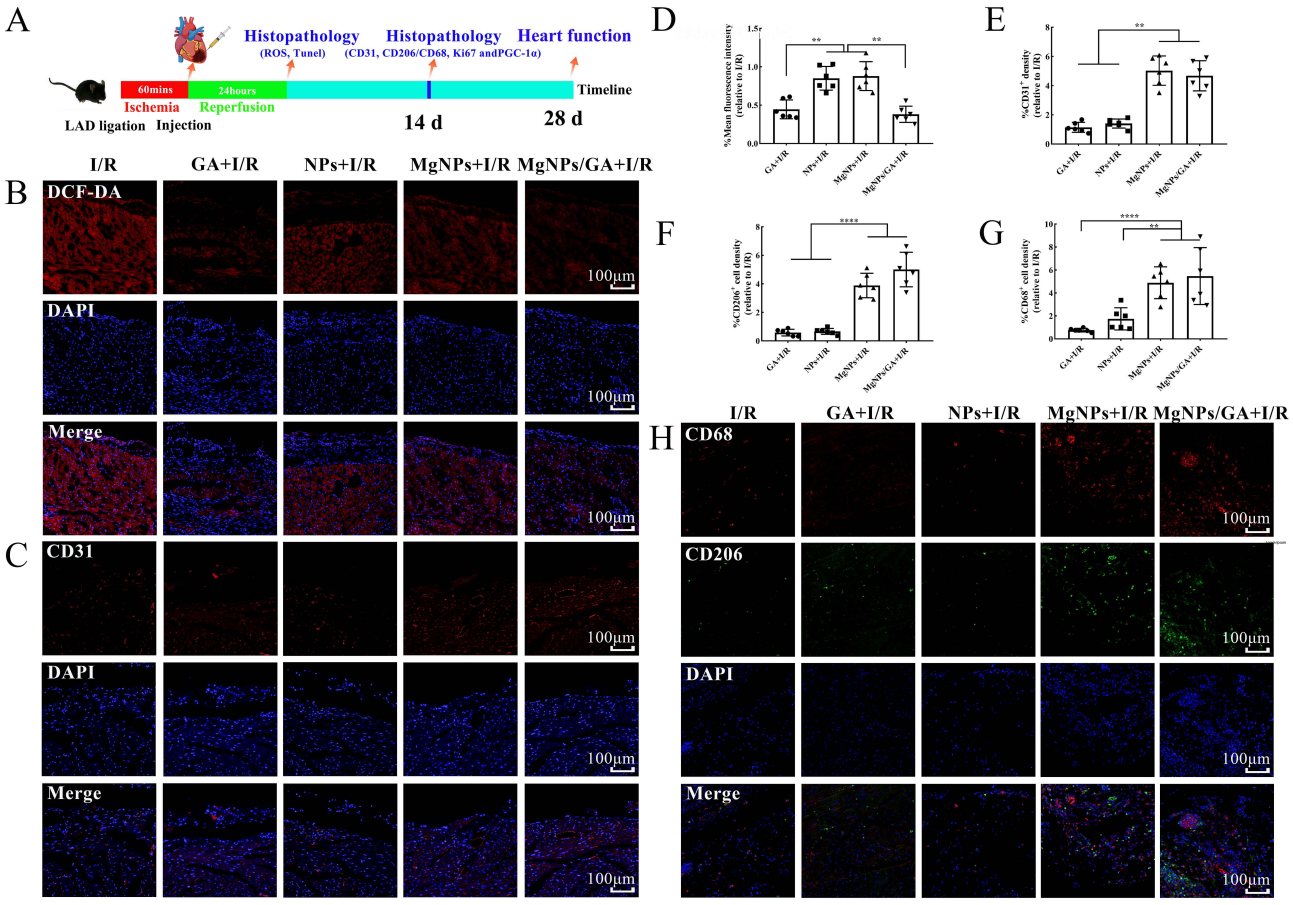

Figure 7 Immunofluorescence staining of histopathological sections after I/R animal model. (**A**) Schematic diagram of the establishment of the I/R mouse model and protocol for evaluating therapeutic effects. (**B**) Detection of reactive oxygen species in the region of injured myocardium 24h after I/R in mice, scale bar: 100μm. (**C**) Detection of Angiogenesis in Areas of Injured Myocardium 14 Days After I/R in mice, scale bar: 100μm. (**D**) Quantitative analysis of ROS fluorescent probe staining of histopathologic sections. (**E**) Quantitative analysis of CD31 immunofluorescence staining of histopathological sections. (**F–H**) The number of M2 macrophages in the region of injured myocardium was detected and quantitatively analyzed 14 days after I/R in mice, scale bar: 100μm. Results are presented as mean ± SD (N = 6), **P < 0.01, ****P < 0.001.

further confirms that MgNPs/GA can effectively scavenge reactive oxygen species and greatly reduce damage to cardiomyocytes. The sustained release of Mg^{2+} promotes tissue vascular regeneration and facilitates macrophage phenotype transformation while reducing the expression of inflammation-related genes. Previous studies have also established that Mg^{2+} promotes tissue vascular regeneration and exerts anti-inflammatory effects,[26] which is consistent with our research findings.

In addition, we examined the hypothesis that GA and Mg^{2+} released from MgNPs/GA could serve as protective components for the ischemic myocardium. Different groups of mice were set up for comparison: the I/R group, GA group, NPs group, MgNPs group, and MgNPs/GA group. As can be seen in Figure 8A, the mortality rate for the I/R group and GA group was 14.3% (1 death out of 7 mice), while no mouse deaths were observed in the NPs, MgNPs, and MgNPs/GA groups during the subsequent 28 days. The body weight of mice in all groups decreased at 24 hours postoperatively and gradually increased thereafter, with no significant differences among the groups (Figure 8B). On day 28 after the mice were operated, we evaluated the infarct area after each group of treated mice by TTC staining (Figure 8C and D). Although the GA and MgNPs groups had some therapeutic effect on I/R mice, the effect was not significant, while the therapeutic effect of MgNPs was significantly higher than that of the other groups. This is due to the fact that the heart is inherently a complex system, and treatment in one aspect alone is not effective in reducing infarct size. Furthermore, compared to the I/R and NPs groups, the left ventricular ejection fraction and left ventricular fractional shortening were significantly improved in the GA, MgNPs, and MgNPs/GA groups (Figure 8E–G). Among them, the MgNPs/GA group showed the most significant improvement, with the lowest end-systolic volume (LVESV) and end-

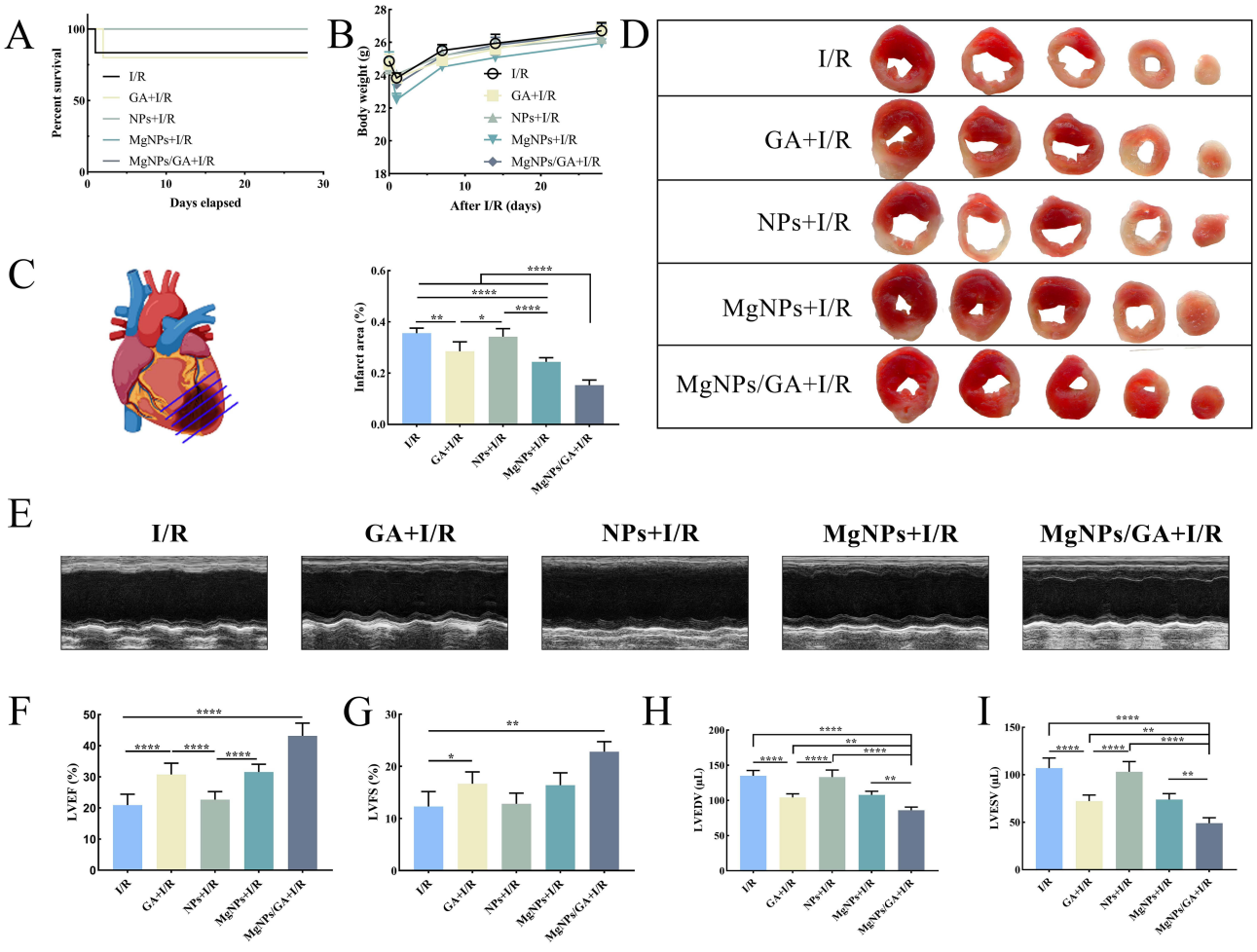

Figure 8 MgNPs/GA Enhances Cardiac Function in I/R Mice. (**A**) Survival curves for each group of mice over 28 days. (**B**) Changes in body weight over 28 days in each group of mice. (**C** and **D**) TTC staining to assess infarct size in I/R mice. (**E–I**) Cardiac function indexes were detected by cardiac ultrasound after 28 days in I/R mice. Results are presented as mean ± SD (N = 6), *P < 0.05, **P < 0.01, ****P < 0.001.

diastolic left ventricular volume (LVEDV) (Figure 8H and I). Our results indicate that GA and Mg^{2+} released from the nanoparticles can enhance heart function after ischemia/reperfusion injury.

Discussion

Myocardial ischemia is an enormous threat to public health and mostly caused by coronary artery thrombosis, which reduces or interrupts blood supply and leads to myocardial cell death. A thorough understanding of the pathological processes involved in the development of the disease is important in designing therapeutic strategies. Myocardial ischemia-reperfusion injury is one of the most common diseases associated with excessive ROS generation,[27] and therefore early antioxidant therapy is considered to be the most promising treatment strategy. In addition to early antioxidant therapy, restoration of blood perfusion is another critical issue in ischaemic myocardial tissue repair.[28] The re-establishment of blood flow in the infarcted tissue can provide sufficient oxygen and nutrients to the cells in the ischaemic area.

Based on the physiopathological environment of the disease, we modified the traditional bioactive glass by removing Ca, a component that can cause calcium overload, and adding Mg to the composition. Subsequently, we loaded gallic acid with antioxidant effects into bioactive glasses with mesoporous structures. Finally, MgNPs/GA with therapeutic effects were synthesised. Our findings indicated that the cumulative release rate of 6% MgNPs/GA was approximately 63.15% (Figure 1I). Generally, the drug loading capacity is closely related to the surface area and pore volume of the nanoparticles. Based on the cumulative-release curves of the nanoparticles, it can be concluded that the incorporation of Mg did not significantly affect the drug release. Furthermore, the structure of the nanoparticles plays a crucial role in drug adsorption, which is commonly achieved through Fickian diffusion. Clearly, the release mechanism of GA from MgNPs is consistent with Fickian diffusion.[29] While GA has strong antioxidant effects as a model drug,[30,31] its therapeutic application is limited by pharmacokinetic defects. Studies involving oral administration of GA in animals showed low bioavailability of this phenolic compound. Although GA absorption is fast, the maximum plasmatic drug concentration reached is low.[32] The use of nanocarriers for drug delivery could be a crucial solution to this challenge. Researchers in various fields have explored different nanoparticles loaded with GA, including poly (lactic-co-glycolic acid) (PLGA) nanoparticles,[33] chitosan nanoparticles,[34] and Silica Nanoparticles.[35] Our findings indicated that the stable release of GA led to a significant decrease in intracellular ROS levels, which also reduced cardiomyocyte apoptosis (Figures 6 and 7B).

Magnesium is one of the essential trace elements in the human body and plays a critically important role in human health. It acts as an activator for numerous enzymes, regulates processes such as cell membrane permeability, cell division, and protein synthesis, and is also involved in the regulation of organ functions, including the heart and neuromuscular system. The stable release of Mg^{2+} can guarantee that there will be no sudden increase in the ion concentration in the body, which can largely avoid cellular dysfunction due to the ion concentration (Figure S1). Mg^{2+} has been demonstrated to promote cell proliferation and angiogenesis.[33–35] Apart from enhancing HUVEC proliferation, magnesium ions also impact multiple-signaling pathways to induce growth factor secretion, such as PDGF and VEGF.[36] Increased secretion of PDGF and VEGF promotes significant endothelial cell proliferation, creating a positive feedback loop. These views align with our results obtained from in vitro and in vivo experiments (Figures 4 and 7C). A previous investigation found that the biological activity of magnesium ions was dose-dependent,[37] although this study did not elucidate whether different concentrations of Mg^{2+} elicited varying responses in HUVECs. Nevertheless, our results provide compelling evidence. In addition, evidence has shown that inadequate magnesium levels are linked to inflammatory response-related pathological conditions. These conditions are characterized by the activation of macrophages, the release of inflammatory cytokines and acute-phase proteins, as well as an excessive generation of free radicals.[38] The type and duration of immune response, as well as the types and duration of cellular reactions involved, can greatly influence the healing outcome of damaged tissues, from fibrosis formation to regeneration.[39,40] Our results indicated that treatment with MgNPs/GA significantly increased the number of M2 macrophages and up-regulated the expression of M2-associated genes, while also significantly reducing pro-inflammatory factors. The density of M2 macrophages at the site of injury is crucial for achieving optimal therapeutic effects.[41–43] Previous studies have suggested that Mg^{2+} exerts anti-inflammatory effects at certain concentrations.[44] Magnesium ions can regulate the inflammatory response through various mechanisms and significantly impact the inflammatory processes. They can inhibit the expression of various inflammation-related factors, such as tumor necrosis factor-alpha (TNF-α), interleukin-1 beta (IL-1β), and interleukin-6 (IL-6).[45]

The cardiac tissue is composed of a multicellular microenvironment, and the interplay between cells is crucial for tissue repair.[46,47–49] Intervening with multiple cells in the pathological environment during disease development to produce beneficial effects may be a highly promising therapeutic concept. Although the therapeutic mechanism was not explored in this study, it is important to explore the therapeutic mechanism of Mg^{2+} by acting on macrophages and endothelial cells simultaneously. The MgNPs/GA proposed in this study ultimately enhance cardiac function by affecting cardiomyocytes, endothelial cells, and macrophages in the context of myocardial ischemia, thereby increasing cardiomyocyte survival, promoting angiogenesis, and facilitating M2 macrophage polarization. All these findings suggest that MgNPs/GA have the potential to be a therapeutic element for impaired cardiac tissues when locally applied in the infarcted myocardium, which may provide a new therapeutic strategy for the treatment of ischemic heart disease.

Conclusions

In this study, magnesium ions were incorporated into mesoporous bioactive glass, and gallic acid was loaded as a model drug into the pores, resulting in the formation of multifunctional nanoparticles. As gallic acid and Mg^{2+} were gradually released, the excessive reactive oxygen species generated during reperfusion injury were cleared. Furthermore, Mg^{2+} promoted vascular regeneration and exerted anti-inflammatory effects. These effects were validated both in vitro and in vivo. Through the utilization of these multifunctional nanoparticles, early production of reactive oxygen species during reperfusion injury can be effectively eliminated, leading to an increased survival rate of cardiomyocytes. Moreover, in the subsequent repair stage, these nanoparticles can accelerate cardiac repair. Our present findings indicate the potential utility of these multifunctional nanoparticles in the therapy of myocardial ischemia-reperfusion injury.

Author Contributions

All authors have made significant contributions to the work reported, including conception, study design, execution, data acquisition, analysis and interpretation, as well as manuscript drafting, revision, and critical review. All authors have provided final approval of the submitted version for publication and have agreed to the journal to which the article has been submitted, with full accountability for all aspects of the work.

Funding

This work was funded by the National Natural Science Foundation of China (grant no. 82270382, 82170505, 82200534), the Natural Science Foundation of Jiangxi Province (grant no. 20204BCJ22028, 20212ACB206020, 20203BBGL73141 and 20192BAB205070), the Natural Science Foundation of Hubei Province (2023AFB817), Key Research and Development Project of Hubei Provincial Department of Science and Technology (2023BCB002), Wuhan Talent's Industry-Leading Talent Project (WHYCCYLJ2021002), the talent Project of Zhongnan Hospital of Wuhan University (grant no. rcyj20210601, xkjs202002, CXPY2022046).

Disclosure

The authors report no conflicts of interest in this work.

References

1. Frantz S, Hundertmark MJ, Schulz-Menger J, et al. Left ventricular remodelling post-myocardial infarction: pathophysiology, imaging, and novel therapies. *Eur Heart J*. 2022;43(27):2549–2561. doi:10.1093/eurheartj/ehac223
2. Caccioppo A, Franchin L, Grosso A, et al. Ischemia reperfusion injury: mechanisms of damage/protection and novel strategies for cardiac recovery/regeneration. *Int J Mol Sci*. 2019;20(20):5024. doi:10.3390/ijms20205024
3. Algoet M, Janssens S, Himmelreich U, et al. Myocardial ischemia-reperfusion injury and the influence of inflammation. *Trends Cardiovasc Med*. 2023;33(6):357–366. doi:10.1016/j.tcm.2022.02.005
4. Zhao T, Wu W, Sui L, et al. Reactive oxygen species-based nanomaterials for the treatment of myocardial ischemia reperfusion injuries. *Bioact Mater*. 2022;7:47–72. doi:10.1016/j.bioactmat.2021.06.006
5. Reiter RJ, Mayo JC, Tan DX, et al. Melatonin as an antioxidant: under promises but over delivers. *J Pineal Res*. 2016;61(3):253–278. doi:10.1111/jpi.12360
6. Ma W, Wei S, Zhang B, et al. Molecular mechanisms of cardiomyocyte death in drug-induced cardiotoxicity. *Front Cell Dev Biol*. 2020;8:434. doi:10.3389/fcell.2020.00434

7. Liu X, Zhang Y, Hong L, et al. Gallic acid increases atrial natriuretic peptide secretion and mechanical dynamics through activation of PKC. *Life Sci*. 2017;181:45–52. doi:10.1016/j.lfs.2017.05.024
8. Zhang S, Luo Y, Zeng H, et al. Encapsulation of selenium in chitosan nanoparticles improves selenium availability and protects cells from selenium-induced DNA damage response. *J Nutr Biochem*. 2011;22(12):1137–1142. doi:10.1016/j.jnutbio.2010.09.014
9. Bheri S, Davis ME. Nanoparticle-hydrogel system for post-myocardial infarction delivery of MicroRNA. *ACS Nano*. 2019;13(9):9702–9706. doi:10.1021/acsnano.9b05716
10. Wang RM, Christman KL. Decellularized myocardial matrix hydrogels: in basic research and preclinical studies. *Adv Drug Deliv Rev*. 2016;96:77–82. doi:10.1016/j.addr.2015.06.002
11. Li L, Wang Y, Guo R, et al. Ginsenoside Rg3-loaded, reactive oxygen species-responsive polymeric nanoparticles for alleviating myocardial ischemia-reperfusion injury. *J Control Release*. 2020;317:259–272. doi:10.1016/j.jconrel.2019.11.032
12. Bae S, Park M, Kang C, et al. Hydrogen peroxide-responsive nanoparticle reduces myocardial ischemia/reperfusion injury. *J Am Heart Assoc*. 2016;5(11). doi:10.1161/JAHA.116.003697
13. Baino F, Hamzehlou S, Kargozar S. Bioactive glasses: where are we and where are we going. *J Funct Biomater*. 2018;9(1):25. doi:10.3390/jfb9010025
14. Perić KŽ, Rider P, Alkildani S, et al. An introduction to bone tissue engineering. *Int J Artif Organs*. 2020;43(2):69–86. doi:10.1177/0391398819876286
15. Kargozar S, Montazerian M, Hamzehlou S, et al. Mesoporous bioactive glasses: promising platforms for antibacterial strategies. *Acta Biomater*. 2018;81:1–19. doi:10.1016/j.actbio.2018.09.052
16. Vargas GE, Haro Durand LA, Cadena V, et al. Effect of nano-sized bioactive glass particles on the angiogenic properties of collagen based composites. *J Mater Sci Mater Med*. 2013;24(5):1261–1269. doi:10.1007/s10856-013-4892-7
17. Lukowiak A, Lao J, Lacroix J, et al. Bioactive glass nanoparticles obtained through sol-gel chemistry. *Chem Commun*. 2013;49(59):6620–6622. doi:10.1039/c3cc00003f
18. Ren G, Li K, Hu Y, et al. Optimization of selenizing conditions for Seleno-Lentinan and its characteristics. *Int J Biol Macromol*. 2015;81:249–258. doi:10.1016/j.ijbiomac.2015.08.012
19. Shi M, Cao X, Zhuang J, et al. The cardioprotective effect and mechanism of bioactive glass on myocardial reperfusion injury. *Biomed Mater*. 2021;16(4):045044. doi:10.1088/1748-605X/ac067e
20. Zheng K, Kang J, Rutkowski B, et al. Toward highly dispersed mesoporous bioactive glass nanoparticles with high Cu concentration using Cu/Ascorbic acid complex as precursor. *Front Chem*. 2019;7:497. doi:10.3389/fchem.2019.00497
21. Wang D, Yao Y, He J, et al. Engineered cell-derived microparticles Bi2Se3/DOX@MPs for imaging guided synergistic photothermal/low-dose chemotherapy of cancer. *Adv Sci*. 2020;7(3):1901293. doi:10.1002/advs.201901293
22. Yoshizawa S, Brown A, Barchowsky A, et al. Magnesium ion stimulation of bone marrow stromal cells enhances osteogenic activity, simulating the effect of magnesium alloy degradation. *Acta Biomater*. 2014;10(6):2834–2842. doi:10.1016/j.actbio.2014.02.002
23. Vannella KM, Wynn TA. Mechanisms of organ injury and repair by macrophages. *Annu Rev Physiol*. 2017;79(1):593–617. doi:10.1146/annurev-physiol-022516-034356
24. Sun K, Li -Y-Y, Jin J. A double-edged sword of immuno-microenvironment in cardiac homeostasis and injury repair. *Signal Transduct Target Ther*. 2021;6(1):79. doi:10.1038/s41392-020-00455-6
25. Pei J, Cai L, Wang F, et al. LPA2 contributes to vascular endothelium homeostasis and cardiac remodeling after myocardial infarction. *Circ Res*. 2022;131(5):388–403. doi:10.1161/CIRCRESAHA.122.321036
26. Ding Z, Cheng W, Liu L, et al. Nanosized silk-magnesium complexes for tissue regeneration. *Adv Healthc Mater*. 2023;12(26):e2300887. doi:10.1002/adhm.202300887
27. Leem YH, Lee KS, Kim JH, et al. Magnesium ions facilitate integrin alpha 2- and alpha 3-mediated proliferation and enhance alkaline phosphatase expression and activity in hBMSCs. *J Tissue Eng Regen Med*. 2016;10(10):E527–E536. doi:10.1002/term.1861
28. Cochain C, Channon KM, Silvestre JS. Angiogenesis in the infarcted myocardium. *Antioxid Redox Signal*. 2013;18(9):1100–1113. doi:10.1089/ars.2012.4849
29. Hu M, Fang J, Zhang Y, et al. Design and evaluation a kind of functional biomaterial for bone tissue engineering: selenium/mesoporous bioactive glass nanospheres. *J Colloid Interface Sci*. 2020;579:654–666. doi:10.1016/j.jcis.2020.06.122
30. Abdelwahed A, Bouhlel I, Skandrani I, et al. Study of antimutagenic and antioxidant activities of gallic acid and 1,2,3,4,6-pentagalloylglucose from Pistacia lentiscus. Confirmation by microarray expression profiling. *Chem Biol Interact*. 2007;165(1):1–13. doi:10.1016/j.cbi.2006.10.003
31. Zhang W, Zeng QM, Tang RC. Gallic acid functionalized polylysine for endowing cotton fiber with antibacterial, antioxidant, and drug delivery properties. *Int J Biol Macromol*. 2022;216:65–74. doi:10.1016/j.ijbiomac
32. Bhattacharyya S, Ahammed SM, Saha BP, et al. The gallic acid-phospholipid complex improved the antioxidant potential of gallic acid by enhancing its bioavailability. *AAPS Pharm Sci Tech*. 2013;14(3):1025–1033. doi:10.1208/s12249-013-9991-8
33. de Cristo Soares Alves A, Mainardes RM, Khalil NM. Nanoencapsulation of gallic acid and evaluation of its cytotoxicity and antioxidant activity. *Mater Sci Eng C Mater Biol Appl*. 2016;60:126–134. doi:10.1016/j.msec.2015.11.014
34. Kaparekar PS, Pathmanapan S, Anandasadagopan SK. Polymeric scaffold of Gallic acid loaded chitosan nanoparticles infused with collagen-fibrin for wound dressing application. *Int J Biol Macromol*. 2020;165(Pt A):930–947. doi:10.1016/j.ijbiomac.2020.09.212
35. Ahangarpour A, Sharifinasab H, Kalantari H, et al. Gallic acid and gallic acid nanoparticle modulate insulin secretion pancreatic β-islets against silica nanoparticle-induced oxidative damage. *Biol Trace Elem Res*. 2022;200(12):5159–5171. doi:10.1007/s12011-022-03111-y
36. Ma J, Zhao N, Zhu D. Biphasic responses of human vascular smooth muscle cells to magnesium ion. *J Biomed Mater Res A*. 2016;104(2):347–356. doi:10.1002/jbm.a.35570
37. Wang J, Xu J, Song B, et al. Magnesium (Mg) based interference screws developed for promoting tendon graft incorporation in bone tunnel in rabbits. *Acta Biomater*. 2017;63:393–410. doi:10.1016/j.actbio.2017.09.018
38. Yuan Z, Wan Z, Gao C, et al. Controlled magnesium ion delivery system for in situ bone tissue engineering. *J Control Release*. 2022;350:360–376. doi:10.1016/j.jconrel.2022.08.036
39. Mazur A, Maier JA, Rock E, et al. Magnesium and the inflammatory response: potential physiopathological implications. *Arch Biochem Biophys*. 2007;458(1):48–56. doi:10.1016/j.abb.2006.03.031

40. Knipper JA, Willenborg S, Brinckmann J, et al. Interleukin-4 receptor α signaling in myeloid cells controls collagen fibril assembly in skin repair. *Immunity*. 2015;43(4):803–816. doi:10.1016/j.immuni.2015.09.005
41. Gieseck RL, Ramalingam TR, Hart KM, et al. Interleukin-13 activates distinct cellular pathways leading to ductular reaction, steatosis, and fibrosis. *Immunity*. 2016;45(1):145–158. doi:10.1016/j.immuni.2016.06.009
42. Wynn TA, Vannella KM. Macrophages in tissue repair, regeneration, and fibrosis. *Immunity*. 2016;44(3):450–462. doi:10.1016/j.immuni.2016.02.015
43. Gieseck RL, Wilson MS, Wynn TA. Type 2 immunity in tissue repair and fibrosis. *Nat Rev Immunol*. 2018;18(1):62–76. doi:10.1038/nri.2017.90
44. Sadtler K, Estrellas K, Allen BW, et al. Developing a pro-regenerative biomaterial scaffold microenvironment requires T helper 2 cells. *Science*. 2016;352(6283):366–370. doi:10.1126/science.aad9272
45. Costantino MD, Schuster A, Helmholz H, et al. Inflammatory response to magnesium-based biodegradable implant materials. *Acta Biomater*. 2020;101:598–608. doi:10.1016/j.actbio.2019.10.014
46. Nielsen FH. Magnesium deficiency and increased inflammation: current perspectives. *J Inflamm Res*. 2018;11:25–34. doi:10.2147/JIR.S136742
47. Chouchani ET, Pell VR, Gaude E, et al. Ischaemic accumulation of succinate controls reperfusion injury through mitochondrial ROS. *Nature*. 2014;515(7527):431–435. doi:10.1038/nature13909
48. Piard C, Jeyaram A, Liu Y, et al. 3D printed HUVECs/MSCs cocultures impact cellular interactions and angiogenesis depending on cell-cell distance. *Biomaterials*. 2019;222:119423. doi:10.1016/j.biomaterials.2019.119423
49. Sack MN, Fyhrquist FY, Saijonmaa OJ, et al. Basic biology of oxidative stress and the cardiovascular system: part 1 of a 3-part series. *J Am Coll Cardiol*. 2017;70(2):196–211. doi:10.1016/j.jacc.2017.05.034